Journal of Magnetic Resonance 343 (2022) 107304

Contents lists available at ScienceDirect

Journal of Magnetic Resonance

journal homepage: www.elsevier.com/locate/jmr

Proton-detected solution-state NMR at 14.1 T based on scalar-driven ^{13}C Overhauser dynamic nuclear polarization

Murari Soundararajan [a], Thierry Dubroca [a], Johan van Tol [a], Stephen Hill [a,c], Lucio Frydman [a,b,*], Sungsool Wi [a,*]

[a] National High Magnetic Field Laboratory, Tallahassee, FL 32310, USA
[b] Department of Chemical and Biological Physics, Weizmann Institute of Sciences, 76100001 Rehovot, Israel
[c] Department of Physics, Florida State University, Tallahassee, FL 32306, USA

ARTICLE INFO

Article history:
Received 24 July 2022
Revised 16 September 2022
Accepted 19 September 2022
Available online 23 September 2022

Keywords:
Overhauser DNP
Hyperpolarization
solution-state NMR
^{1}H NMR
Heteronuclear correlations

ABSTRACT

Overhauser dynamic nuclear polarization (ODNP) NMR of solutions at high fields is usually mediated by scalar couplings that polarize the nuclei of heavier, electron-rich atoms. This leaves ^{1}H-detected NMR outside the realm of such studies. This study presents experiments that deliver ^{1}H-detected NMR experiments on relatively large liquid volumes (60 ~ 100 μL) and at high fields (14.1 T), while relying on ODNP enhancements. To this end ^{13}C NMR polarizations were first enhanced by relying on a mechanism that utilizes e^{-}-^{13}C scalar coupling interactions; the nuclear spin alignment thus achieved was then passed on to neighboring ^{1}H for observation, by a reverse INEPT scheme relying on one-bond J_{CH}-couplings. Such $^{13}C \rightarrow {}^{1}H$ polarization transfer ported the ^{13}C ODNP gains into the ^{1}H, permitting detection at higher frequencies and with higher potential sensitivities. For a model solution of labeled $^{13}CHCl_3$ comixed with a nitroxide-based TEMPO derivative as polarizing agent, an ODNP enhancement factor of ca. 5x could thus be imparted to the ^{1}H signal. When applied to bigger organic molecules like 2-^{13}C-phenylacetylene and $^{13}C_8$-indole, ODNP enhancements in the 1.2-3x range were obtained. Thus, although handicapped by the lower γ of the ^{13}C, enhancements could be imparted on the ^{1}H thermal acquisitions in all cases. We also find that conventional ^{1}H–^{13}C nuclear Overhauser enhancements (NOEs) are largely absent in these solutions due to the presence of co-dissolved radicals, adding negligible gains and playing negligible roles on the scalar $e^{-} \rightarrow {}^{13}C$ ODNP transfer. Potential rationalizations of these effects as well as extensions of these experiments, are briefly discussed.

1. Introduction

NMR is a powerful analytical tool to investigate the structure and dynamics of molecules in solutions. Despite its advantages, NMR suffers from an intrinsically poor sensitivity reflecting weak magnetic interactions that lead to small spin polarizations and, sometimes, from a low natural abundance of the NMR active nucleus of interest. Dynamic Nuclear Polarization (DNP) is an effective and versatile technique that can be used to increase NMR's sensitivity; DNP takes advantage of an electron's large gyromagnetic ratio, and transfers its intrinsically larger polarization to nuclei for their NMR investigation [1–2]. However, while the high efficiencies of electron → nucleus polarization transfer mechanisms at cryogenic temperatures have enabled DNP to revolutionize solids and *in vivo* metabolic NMR [3–13], solution-state NMR has not seen comparable successes yet – particularly when executed at the high magnetic fields of interest in analytical spectroscopy. Liquid state DNP operates primarily through the Overhauser DNP (ODNP) mechanism, whereby a free radical dissolved in solution exhibits fluctuating interactions between the paramagnetic electrons and the target nuclei under NMR investigation [14]. When the electron spin polarization is perturbed away from equilibrium, for instance by the continuous application of microwave (MW) irradiation at its Larmor frequency, these time-dependent interactions lead to a cross-relaxation between the electron and the coupled nuclei of interest, eventually transferring the electron spin polarization to the nucleus [15]. The extent of this ODNP enhancement will depend on both the degree of saturation imparted on the electron spin resonance (ESR) line, and on the efficiency of the electron/nuclear cross-relaxation. These processes can become significantly inefficient as the targeted solution is studied in increasing magnetic fields. On the hardware side, the main obstacle to high-field solution-state ODNP is the requirement

* Corresponding authors.
E-mail addresses: lucio.frydman@weizmann.ac.il (L. Frydman), lucio.frydman@weizmann.ac.il, sungsool@magnet.fsu.edu (S. Wi).

https://doi.org/10.1016/j.jmr.2022.107304
1090-7807/

for ever higher MW powers for saturating the ESR line(s): a typical sample, prepared based on nitroxides as ODNP polarizing agents, will require ~ 0.2 mT B_1 fields to achieve this saturation at high fields [16]. Reaching such B_1 values requires the use of microwave resonant cavities [17–18], or high power sources such as gyrotrons [19–21]. Resonant cavities overcome the necessity of using a high MW power, but restrict the sample volumes to sub-microliter ranges and add significant complexity to the radiofrequency (RF) resonator design, making it difficult to integrate multiple RF channels while maintaining a high efficiency [22–23]. On the other hand, the use of high powers may enable the utilization of a conventional liquid-state NMR probe-head that allows the use of a large sample volume. However, unless special provisions are taken, this method cannot avoid inducing substantial sample heating [24]. An even more fundamental challenge is posed by the lack of efficiency of the electron-nucleus cross-relaxation at high magnetic fields [25]. Improving this requires tailoring the solution state dynamics to match ever shorter time scales, demanding for instance the use of supercritical fluids as low-viscosity solvent media [19,26]. Alternatively, an ODNP-efficient cross relaxation can be found in radical-target combinations where the free electron is effectively coupled to specific nuclear sites on the target molecule via contact hyperfine interactions [17–31]. While strongly site-specific, the ODNP mechanism that relies on this e^--nucleus contact hyperfine interaction has been shown to remain significant even at high magnetic fields [17,20,23,30–31]. This mechanism is based on scalar interactions that require significant electron densities localized, albeit transiently, in the polarized nucleus. Because of this, scalar ODNP enhancements have been reported for heavier species such as ^{13}C, ^{31}P, ^{19}F and ^{15}N [17,20,24,27], but leaves outside their realm ^1Hs, the species with highest intrinsic sensitivity out of all conventionally observed NMR nuclei.

This situation is not exclusive to scalar-based solution-state ODNP: Numerous hyperpolarization methods have emerged, where ^{15}N or ^{13}C species can be efficiently polarized, but ^1H counterparts will either not polarize or not maintain their polarization sufficiently long for enabling meaningful measurements. Given the advantages resulting from relying on the bigger gyromagnetic ratio of ^1Hs, a number of experiments have been recently reported whereby dissolution DNP [32–35], CIDNP [36], or PHIP/PASADENA [37] experiments, are complemented for transfers to ^1H for an enhanced detection. These transfers could happen spontaneously [38] or, more commonly, via J(^{15}N-^1H)- or J(^{13}C–^1H)-based polarization transfers [39–41], leading to an additional gain in sensitivity and occasionally in resolution as well [32–38]. This work is based on a similar concept, but for polarization enhancements that rely on scalar-driven ODNP on ^{13}C species on large volumes and at high fields. These experiments are demonstrated on model solutions containing $^{13}CHCl_3$, 2-^{13}C-phenylacetylene and $^{13}C_8$-indole, which are enhanced by ODNP using TEMPO as the polarizing radical. When passing this ODNP-enhanced ^{13}C polarization to directly bonded ^1Hs by reverse insensitive nuclei enhanced by polarization transfer (rINEPT) schemes, signal increases of ca. 5-fold are achieved on the ^1H spectrum when compared with microwave-less acquisitions. Double-resonance investigations also clarify the role of the protons in the $e^-\rightarrow{}^{13}C$ DNP transfers. These approaches make a suitable starting point to exploit ODNP enhancements on ^1H NMR, as well as to build 2D liquid-state NMR experiments at high magnetic fields. It is worth remarking that while this study was undergoing peer review, a similar study relying on hardware developed for solid state DNP NMR at 400 MHz and smaller samples was reported by Rao et al. [50].

2. Experimental details

ODNP NMR experiments were performed in a 14.1 T Oxford magnet interfaced to a Tecmag Redstone NMR console configured for ^1H operation at 600 MHz. A Bruker-CPI second-harmonic 395 GHz gyrotron was used as a high-power MW source, with a quasi-optical bench to control beam power and polarization, and a shutter to rapidly switch the MW irradiation on and off [24]. The MW power used in all ODNP experiments presented in this work was 13 W. The probe used in the experiments is based on a Varian HX 600 MHz direct-detect broadband 5 mm solution state NMR probe, modified with a customized sweep coil for targeting various radicals, as described in a previous publication [27]. The probe was fitted with a smooth-walled microwave waveguide that replaced the probe's original glass Dewar (Fig. 1a), and ended up at the coil deck with a custom-designed spline-profile horn, shining a TE11 mode MW beam with a 3 mm diameter directely at the sample located inside the NMR coils. Unlike an earlier design were this "sample-waveguide" completely enclosed the sample tube throughout the working length of the NMR coils, [27] the new design uses the sample and sample tube as a dielectric waveguide to contain the MW beam (Fig. 1b). Just below the sample, the TE11 mode waveguide was cut horizontally with multiple slots with a spacing optimized to increase the efficiency of the radiofrequency irradiation at the sample while minimizing the MW transmission losses at 395 GHz. These slots also serve as a path for flowing a stream of nitrogen gas to cool the sample, delivered from the bottom of the probe through the MW waveguide, thus helping to reduce the microwave heating. This design allows us to simultaneously tune both RF channels (^1H and X, where X = ^{31}P, ^{13}C or ^{15}N) for double resonance experiments, while allowing an efficient microwave irradiation on the sample. The sample tube is made of fluorinated ethylene propylene (FEP), a material transparent to microwaves. The index of refraction of FEP is about 1.5 [42], similar to that of typical NMR solvents; this index is larger than that of the surrounding air (≈ 1), allowing the sample-FEP tube combination to act as a dielectric waveguide for the microwaves. A MW nutation measurement using an in-situ pulsed EPR spectrometer on the same setup [27], yielded a peak MW magnetic field of 4.75 μT (133 kHz) with a 7 mW source power, corresponding to a B_1 ≈ 0.2 mT (5.6 MHz nutation frequency) at the gyrotron-supplied MW power. Figs. 1c, 1d show ^{13}C and ^1H nutation curves measured using this custom-designed double-resonance ODNP NMR probe; well-defined 10 μs and 24 μs 90° excitation pulses were exhibited for the ^{13}C and ^1H channels for ca. 120 and 50 W RF powers, respectively. Based on these nutation behaviors we estimate 8 % and 14 % deviations ($I_{9\pi/2}/I_{\pi/2}$ = 0.92 and 0.86, respectively) [47] in the RF homogeneity over the full sample for the ^{13}C and ^1H channels, respectively, confirming essentially no disturbances from the waveguide components or the sweep coil, on the RF performance of the probe.

Sample solutions containing a variety of target molecules –$^{13}CCl_4$, $^{13}CHCl_3$, 2-^{13}C-phenylacetylene and $^{13}C_8$-indole– were chosen to examine the ODNP-driven ^{13}C signal enhancements. These compounds probe the $e^-\rightarrow{}^{13}C$ ODNP phenomenon on ^1H–^{13}C moieties with sp^3, sp^2 and sp hybridizations, all of which have been shown to exhibit ^{13}C NMR enhancements as driven scalar ODNP. [23,29,43–45] The sample solutions formulated for the DNP experiments were as follows: (1) a mixture of 2 % v/v $^{13}CHCl_3$, 8 % v/v $^{13}CCl_4$ and 10 mM 2,2,6,6 tetramethylpiperidinyloxy (TEMPO) radical in 100 μL hexane-d_{14}; (2) a solution of 0.32 M 2-^{13}C-phenylacetylene and 10 mM TEMPO in 60 μL *n*-heptane-d_{16}/toluene d_8 (v/v = 3/1); (3) a solution of 0.44 M $^{13}C_8$-indole

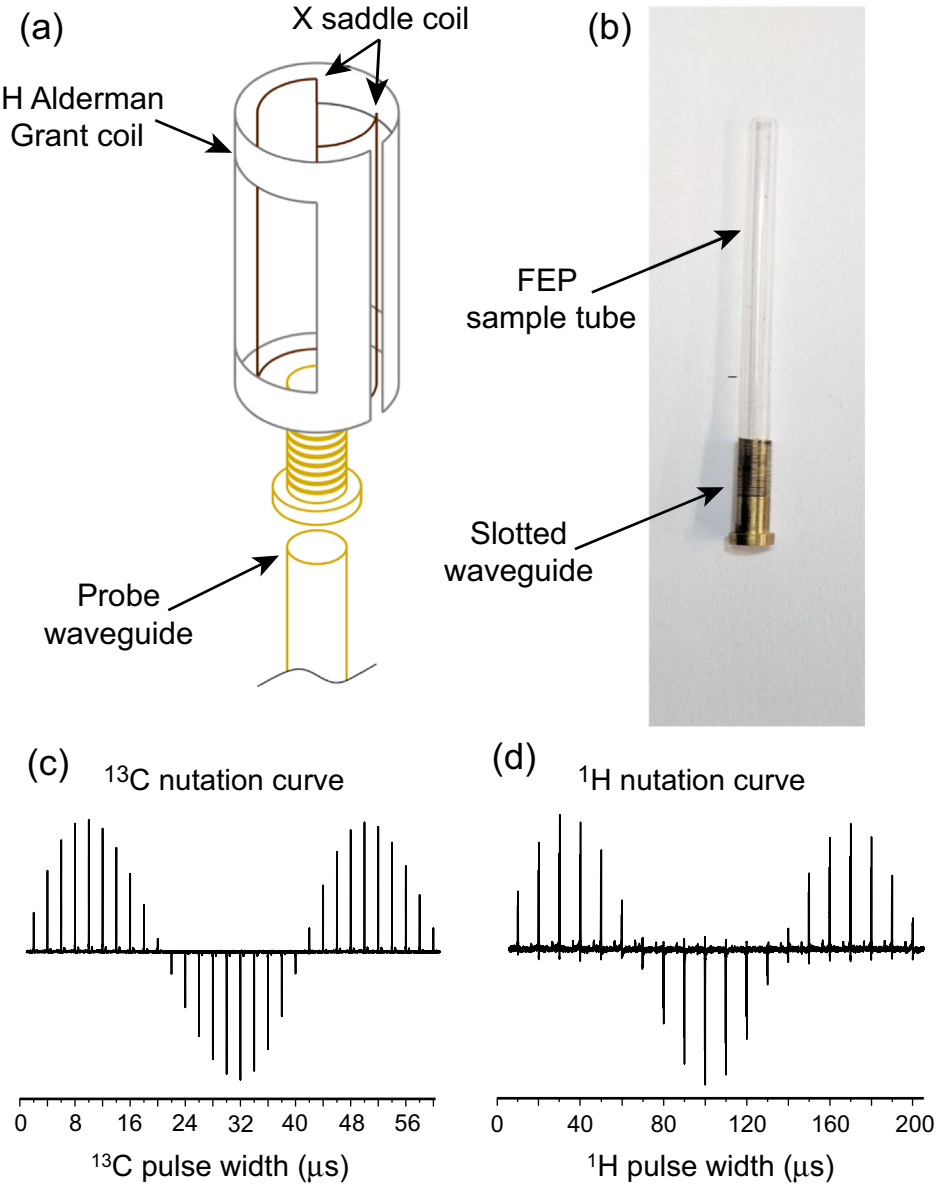

Fig. 1. (a) Schematic of the customized ^{1}H-X double-resonance ODNP NMR probe-head used in this work, highlighting the smooth-walled probe waveguide used to channel the Gyrotron beam to the sample, the slotted waveguide, and the RF coils. During DNP the samples are cooled by a nitrogen gas stream flowing through the waveguide. (b) Slotted waveguide with FEP sample tube partially inserted into it; during experiments the FEP tube sits inside the 2.5 cm long NMR coils. (c, d) ^{13}C and ^{1}H nutation measurements carried out on a sample of 25 % $^{13}CHCl_3$ and 10 mM TEMPO in $^{13}CCl_4$, using the double-resonance ODNP probe.

and 10 mM TEMPO in 60 µL *n*-heptane-d_{16}/p-xylene-d_{10} (v/v = 4/1). All these solutions were based on non-polar solvents such as hexane and heptane that are relatively transparent to microwaves; a minimum amount of toluene or p-xylene was added as an auxiliary solvent to ensure the solubility of phenylacetylene and indole, respectively. All these compounds were purchased from Sigma-Aldrich and used as purchased. These sample solutions were pipetted into 3 mm OD / 2 mm ID FEP tubes for the experiments, that were either welded shut or closed with a Teflon cap for the DNP NMR experiments. All solutions were deoxygenated by performing 5 freeze–pump-thaw cycles under Ar gas environment before preparation; additionally, the filled sample tubes were stored in a glove box for 2 or 3 days under an Ar environment to allow any dissolved oxygen to diffuse out of the solution; the cooling nitrogen gas (vide supra) prevented any oxygenation during the experiments themselves. The 10 mM TEMPO concentration used in these tests came out of a series of optimization studies, where the efficiency of the scalar ODNP was high enough to allow us relatively short MW CW irradiation times (thereby limiting MW-induced heating), while leaving a long enough nuclear T_1 time to enable an efficient polarization. Radical concentrations were verified using a Bruker EMXnano EPR spectrometer before carrying out the ODNP experiments.

Fig. 2 shows the NMR pulse sequences used in this work. Directly polarized ^{13}C or ^{1}H NMR spectra were acquired using a single 90° pulse or a 90°-τ-180°- τ Hahn echo sequence (to eliminate a ca. 10 µs ringdown time ascribed to the presence of the metallic waveguide and potential ^{1}H or ^{13}C background signals), with or without ^{1}H or ^{13}C decoupling (Fig. 2a). WALTZ-16 [46] was used as ^{1}H- or ^{13}C-decoupling sequences; 4.5 kHz nutation fields were used for ^{1}H decoupling and 7.1 kHz for ^{13}C. The e^--^{13}C ODNP effect was initiated by turning on the MW irradiation for a time d_2 before applying the RF pulses. To limit sample heating, the gyrotron beam was gated "on" using a mechanical shutter over

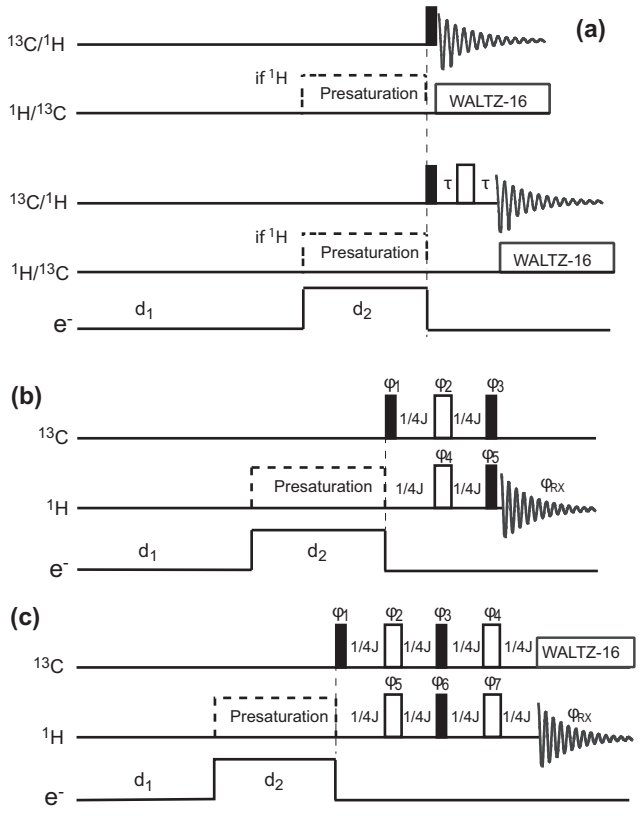

Fig. 2. ODNP NMR pulse sequences employed in this study. Black rectangular bars represent 90° pulses, and empty rectangular bars represent 180° pulses. Microwave gating was turned on for a delay time d_2 prior to the application of RF pulse(s), and turned off for all other periods including d_1, acting as recycling delay. A ^{1}H presaturation pulse was sometimes applied prior to the 90° ^{13}C excitation pulse for probing a putative NOE enhancement of the signals. Shown are pulse sequences for (a) direct ^{13}C observation with ^{1}H decoupling (with or without spin-echo); (b,c) indirect ^{1}H observation via a $^{13}C\rightarrow^{1}H$ rINEPT signal transfer. Shown in (c) is the refocused $^{13}C\rightarrow^{1}H$ rINEPT sequence with ^{13}C decoupling. Delays in (b,c) were tuned to $1/4J(^{13}C–^{1}H)$. Phase cycling: (b) φ_1=(x)8,(-x)8; $\varphi_2 = \varphi_4$ = x,-x; φ_3=(x)4,(y)4,(-x)4,(-y)4; φ_5 = y,y,-y,-y; φ_{Rx} = x,x,-x,-x,y,y,-y,-y. Phase cycling in (c) φ_1=(x)8,(-x)8; $\varphi_2 = \varphi_4 = \varphi_5$ = x,-x; φ_3 = y,y,-y,-y; φ_6=(x)4,(y)4,(-x)4,(-y)4; φ_7=(x,-x)2,(y,-y)2; φ_{Rx} = x, x,-x,-x,y,y,-y,-y.

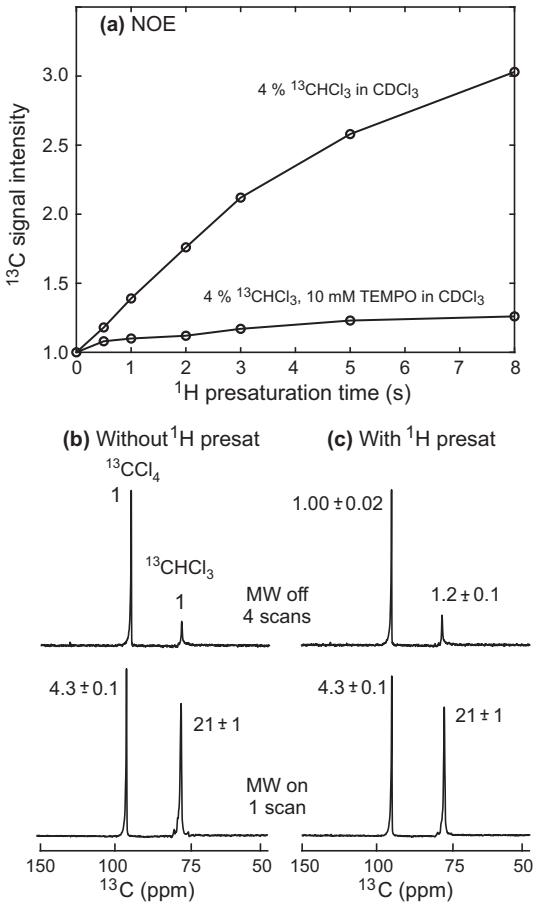

Fig. 3. NOE and ODNP effects examined on $^{13}CHCl_3$ with and without ^{1}H presaturation / MW irradiation. (a) NOE effects measured on 4 % $^{13}CHCl_3$ in $CDCl_3$ with and without adding 10 mM TEMPO. (b,c): ^{13}C NMR spectra obtained on 2 % $^{13}CHCl_3$, 8 % $^{13}CCl_4$, and 10 mM TEMPO in 100 μL hexane-d_{14} without (b) and with (c) ^{1}H presaturation while turning "off" (center) or "on" (bottom) the MW irradiation. The "off" spectra were acquired with 4 scans and the "on" spectra with 1 scan. Signal enhancement factors were estimated with respect to the "off" spectrum without ^{1}H presaturation (areas for each resonance set to 1). The ppm scale was calibrated using the $^{13}CHCl_3$ peak (77 ppm), measured with ^{1}H decoupling and without microwaves on a TEMPO-free sample.

typical d_2 times of 1 to 2 s prior to the application of any NMR pulse; this gate was turned "off" during the RF pulses, the signal acquisition period, and the recycling delay time d_1 (5 to 20 s). The "on" MW irradiation time was adjusted based on the T_1 relaxation time of the polarized nuclei, while the d_1 time was chosen relatively long in order to minimize sample heating. In all cases presented here, peak broadening or shifting due to excessive heat absorption did not occur under any condition. ^{1}H presaturation with a 10 kHz RF field was occasionally applied to examine the potential presence of $^{1}H–^{13}C$ nuclear Overhauser enhancement (NOE) effects. The ^{13}C signals enhanced by ODNP were also observed indirectly via J-coupling mediated rINEPT $^{13}C\rightarrow^{1}H$ sequences (Fig. 2b and 2c), whose echo times were adjusted to $1/4J(^{1}H–^{13}C)$.

3. Results

Before discussing the potential of $^{13}C\rightarrow^{1}H$ transfers under ODNP, we consider it worth examining the extent of the conventional $\{^{1}H\}$-^{13}C NOE effect. 4 % $^{13}CHCl_3$ solutions in $CDCl_3$ with and without 10 mM TEMPO were thus treated with identical cycles of freeze–pump-thaw deoxygenation, and the NOE effect examined under Ar gas environments. In the absence of TEMPO a $\{^{1}H\}$-^{13}C NOE signal enhancement factor of 3 was observed after ≈8 s ^{1}H presaturation, which is the theoretically expected value [48]: $\eta = (I-I_0)/I_0 \approx 3$, where I and I_0 are signal intensities measured with and without ^{1}H presaturation, respectively. However, in the presence of 10 mM TEMPO, the NOE effect was greatly reduced, leaving a residual enhancement of 1.2 (Fig. 3a), with everything else being equal. Fig. 3b and Fig. 3c, respectively, show ^{13}C NMR spectra acquired on this TEMPO-containing sample with and without ^{1}H presaturation, under thermal equilibrium and under ODNP-enhanced conditions. Upon irradiating the sample with microwaves at 395 GHz both the $^{13}CCl_4$ and $^{13}CHCl_3$ signals were enhanced, with ODNP enhancement factors $\varepsilon \approx 4.3 \pm 0.1$ and 21 ± 1, respectively (enhancements were always calculated using areas of the integrated peaks). As reported in the literature the ^{13}-$CHCl_3$ carbon, possessing a directly-bonded ^{1}H, displays an ODNP enhancement that is significantly greater than that of the protonless $^{13}CCl_4$ –apparently because the ^{1}H enables a hydrogen-bond-like connection with the radical facilitating the e^--^{13}C scalar coupling interaction [44–45]. As also shown in Fig. 3, the ODNP signal enhancement detected for the chloroform ^{13}C remains at about 21 (for 13 W MW powers and d_2 = 2 s) regardless of the presence or absence of ^{1}H presaturation. This confirms that the $^{1}H–^{13}C$ cross relaxation, which is a mutual process, can be disregarded when

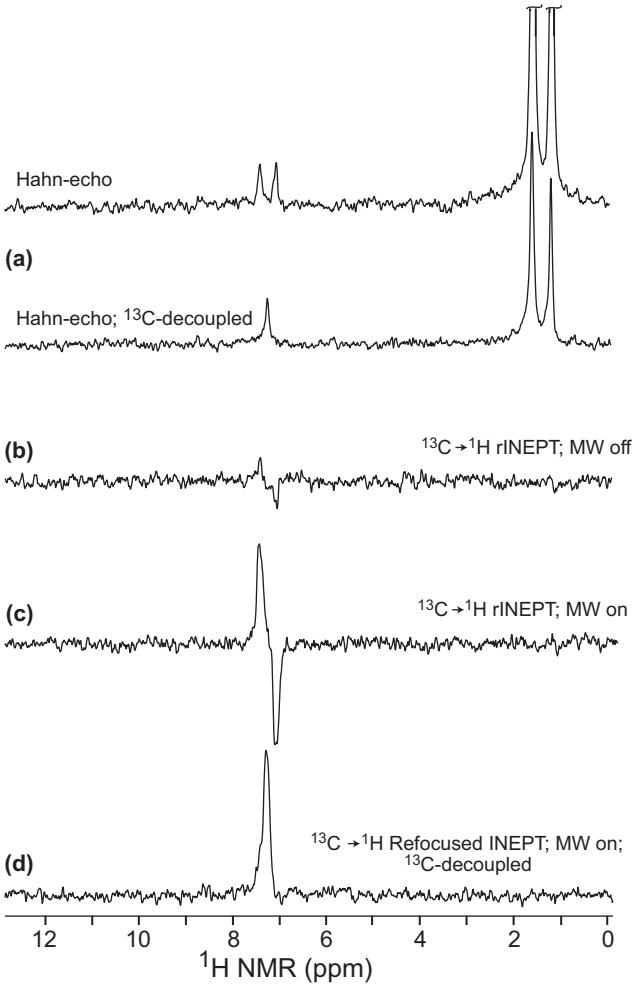

Fig. 4. ^{1}H NMR spectra measured on a $^{13}CCl_4/^{13}CHCl_3$ in the same hexane-d_{14} solution as used in Fig. 3. (a) Thermally polarized ^{1}H spectra with ^{13}C WALTZ-16 decoupling; peaks at 1–2 ppm arise from residual hexane ^{1}Hs. (b-d) ^{1}H signals transferred from the ^{13}C in $^{13}CHCl_3$ upon utilizing $^{13}C \rightarrow {}^{1}H$ rINEPT (Fig. 2b and 2c) without (b) and with (c, d) microwave irradiation. 16 scans were used in every case. The $1/4J(^{1}H–^{13}C)$ delay time used in the rINEPT sequence was set for $J(^{1}H–^{13}C) = 130$ Hz.

the targeted molecule is comixed in solution with ≈10 mM of a radical acting as much more efficient relaxation sink.

Fig. 4 illustrates the outcome of applying the various sequences illustrated in Fig. 2 on the $^{13}CHCl_3/^{13}CCl_4$ solution, when focusing on ^{1}H NMR acquisitions. Shown on top as an initial reference are thermally polarized ^{1}H NMR spectra acquired with and without ^{13}C decoupling (Fig. 4a). These ^{1}H signals showed some broadening but virtually no change in intensity upon MW irradiation, reflecting the unfavorable coupling of TEMPO to protons at high fields[30] and the absence of meaningful $e^{-}–^{1}$H DNP interactions (spectra not shown). Applying the rINEPT sequence on this ^{13}C-labeled solution cleans up the residual solvent resonances in the 1–2 ppm region, but imparts a significant sensitivity penalty by virtue of the ^{13}C's lower thermal polarization under these conditions (Fig. 4b). By contrast, when relying on the ^{13}C ODNP enhancement, the indirectly-polarized ^{1}H can be obtained with a significant sensitivity enhancement vs its thermal counterpart, via a $^{13}C \rightarrow {}^{1}H$ rINEPT block (Fig. 4c); a slightly larger ^{1}H enhancement is observed when employing the refocused INEPT scheme and ^{13}C decoupling, even if the longer time required by this module robs the decoupling from its full potential: the ideal sensitivity of the refocused ^{13}C-decoupled rINEPT in Fig. 4d should be twice that observed in Fig. 4c, while the actual enhancement is only ≈1.5x. This reflects in part the relatively short ^{1}H T_2 of this radical-doped chloroform sample. Still, the ODNP enhancement factor observed in these ^{1}H-detected experiment was ca. 5x when compared with the ^{1}H thermal acquisition, and ca. 20x when compared with the rINEPT ^{1}H spectrum obtained if starting from thermal ^{13}C polarization. Considering that the gyromagnetic ratios of ^{13}C and ^{1}H differ by a factor of 4 these observed enhancement factors are reasonable, and indicate a good efficiency for the $^{13}C \rightarrow {}^{1}H$ rINEPT transfer.

Fig. 5 presents a similar series of e^{-}-$^{13}C–^{1}H$ scalar-coupling ODNP NMR experiments, performed on a 0.32 M 2-^{13}C-phenylacetylene, 10 mM TEMPO solution in 60 μL heptane-d_{18}/toluene d_8 (v/v = 3/1) (this amount of toluene d_8 added to better solubilize phenylacetylene in heptane-d_{16}). As in the chloroform case this sample was deoxygenated by freeze–pump-thaw under Ar, and kept in a N_2 gas stream (precooled to −20 °C) during the ODNP experiments. Also as in the chloroform case, the NOE effect arising on the ^{13}C upon presaturating ^{1}Hs in this sample was much below the maximum theoretical value: about a 1.3x enhancement was detected, both when observing ^{13}C directly and when observing the signal transferred to ^{1}H from the ^{13}C following a rINEPT module (Fig. 5a/5b and 5f/5g). ^{13}C ODNP enhancement on the *C*2 of this molecule was ≈10.5x, and varied negligibly within the margin of error (estimated from 3 independent measurements) and/or if adding ^{1}H NOE by presaturation to the MW irradiation (Fig. 5c, 5d). MW irradiation again had no effect on the ^{1}H NMR spectrum of this solution, but ^{1}H spectra monitoring the ^{13}C ODNP effect indirectly via rINEPT transfers (Fig. 5h/5i) showed a 9x increase vs MW-free acquisitions. These ODNP enhancements were identical regardless of whether ^{1}H presaturation was or was not used, and amounted to a ca. 2x gain in the ^{1}H signal sensitivity when compared to the thermal ^{1}H spectrum (Fig. 5e with ^{13}C decoupling). This observation is again consistent with the ODNP enhancements observed for ^{13}C, as $\varepsilon \approx 10.5 \cdot \gamma_C / \gamma_H \approx 2.6$ would be the maximum possible ^{1}H enhancement, with the difference probably reflecting losses over the course of the transfer.

Fig. 6 presents a final example of ^{13}C- and ^{1}H-detected ODNP NMR experiments, measured on a 0.44 M $^{13}C_8$-indole and 10 mM TEMPO solution in 60 μL heptane-d_{16}/p-xylene-d_{10} (v/v = 4/1). As all carbons in this compound were labeled, a variety of enhancements can be seen in this sample –even if at the price of having multiple homonuclear $J_{C\text{-}C}$ couplings complicating the spectra. As in the previous cases, the $\{^{1}H\}$-^{13}C NOE enhancements upon ^{1}H presaturation are relatively modest, ranging from none for quaternary carbon C9, to ca. 1.4x for methine carbon C6. Site-specific enhancements are also a feature of the ODNP-enhanced ^{13}C NMR, with gains ranging from ≈1x for C9, to ≈3x for methine carbons C3 and C6. Once again, addition of a $\{^{1}H\}$-^{13}C NOE effect does not add significantly to these $e^{-} \rightarrow {}^{13}C$ ODNP enhancements, with marginal enhancements adding to the ODNP upon turning on a concurrent ^{1}H presaturation. All these site-specific signal enhancements are transferred in a nearly one-to-one fashion upon indirectly observing them on the ^{1}H NMR spectra, receiving the individual ^{13}C polarizations via rINEPT transfers from their directly-bonded neighbours (Fig. 6, right-hand column).

4. Discussion and conclusions

The present study explored the effects of heteronuclear NOEs and of scalar-coupling-mediated ODNP ^{13}C polarization enhancements, on organic solutions of several compounds ($^{13}CHCl_3$, 2-^{13}C-phenylacetylene, $^{13}C_8$-indole) codissolved with TEMPO. The potential of transferring these enhanced ^{13}C signals to ^{1}Hs for final detection with the aid of rINEPT-based experiments, was also explored. These experiment require a custom-designed solution-state $^{1}H–^{13}C$-electron multiple-resonance DNP setup, capable of

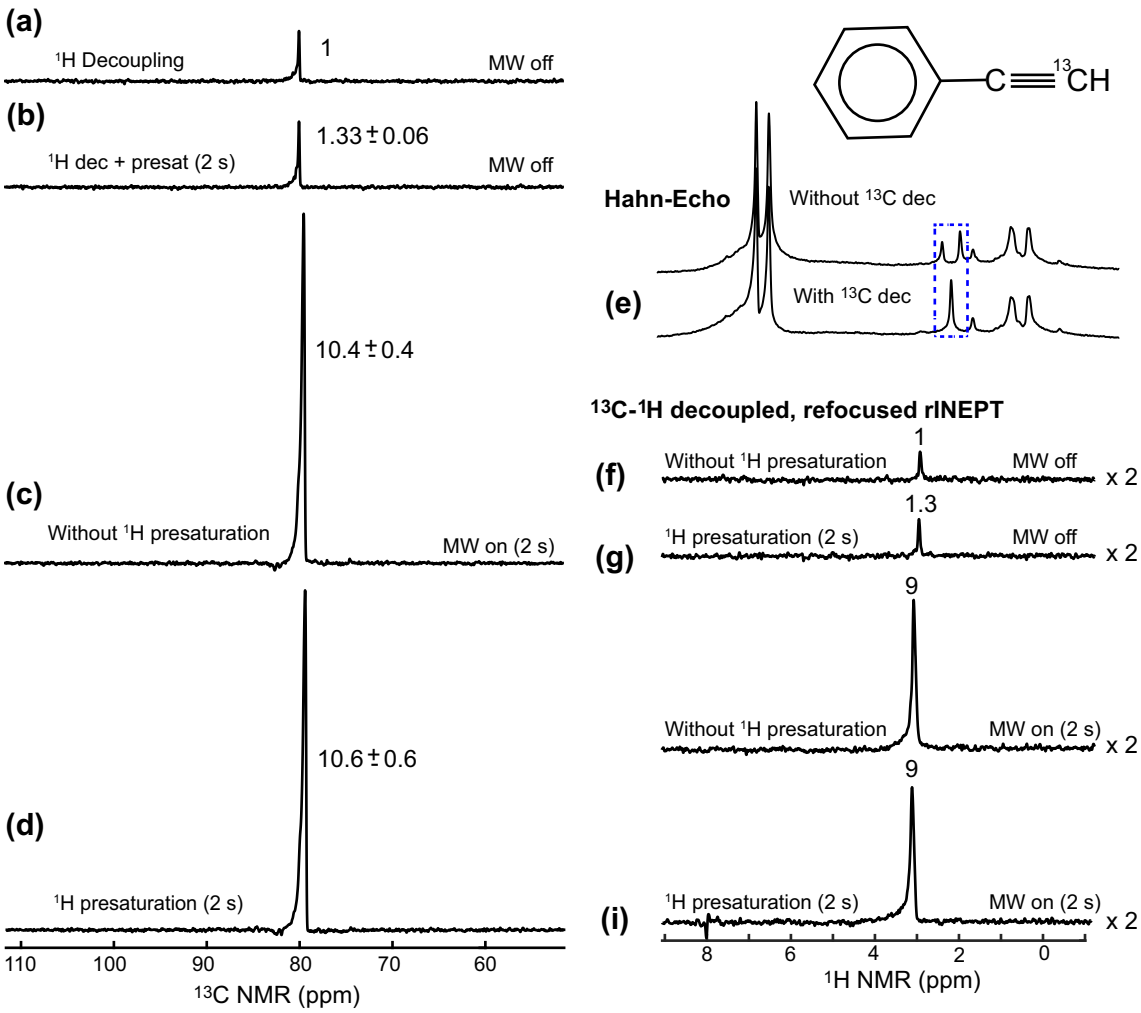

Fig. 5. ^{13}C (a-d) and ^{1}H (e-i) NMR data measured for a 2-^{13}C-phenylacetylene, 10 mM TEMPO in 60 μL heptane/toluene solutions under a variety of NOE (^{1}H presaturation) and $e^- \rightarrow {}^{13}$C ODNP conditions, as specified in each panel. Shown in panels (f-i) are reversed INEPT ^{1}H spectra acquired assuming a $J(^1H–^{13}C) = 240$ Hz. All spectra were acquired by co-adding 16 scans for signal averaging with $d_1 = 20$ s; all ppm scales were adjusted according to the literature data [43]. Full-widths at half-heights (FWHH) for the ^{13}C with and without MW irradiation were 23 Hz and 70 Hz, respectively; those for ^{1}H with and without MW were 31 Hz and 36 Hz, respectively. Note that different receiver gain factors were used in measuring the ^{1}H spectra: gain for (e) was twice as for (f-i). Numbers indicate relative peak areas stemming from taking thermal $^{13}C/^1H$ {$^1H/^{13}C$}-decoupled intensities of unity.

delivering quality RF pulses and intense MW fields, without compromising on the abilities of the solution NMR acquisitions. Further, these acquisitions were assayed using relatively large (60 ∼ 100 μL) sample volumes, while operating at high magnetic fields (14.1 T) of analytical interest. As a result of all these demands, the ODNP enhancements reported in this study were not as high as they could be: for instance in our previous publication, employing nearly the same setup and this study, [24] $e^- \rightarrow {}^{13}$C ODNP enhancements of up to ∼ 80 were reported for $^{13}CHCl_3$ –as opposed to the ≈20x enhancement reported here. The previous study, however, used higher MW powers and longer MW irradiation times; these conditions caused heating and temperature gradients in the sample, leading to substantial peak broadening and a significant loss in spectral resolution [24]. Such broadenings would have made meaningless the acquisition of ^{1}H NMR data, characterized as they are by a much narrower ppm range than its heteronuclear counterpart. A sweet spot was therefore sought where good resolution and significant ODNP enhancements, could be simultaneously achieved. The experimental results shown in Figs. 3-6 evidence such achievements, with ^{1}H-decoupled ^{13}C FWHHs increasing by under 50 % and showing negligible chemical shift displacements after 2 s of ≈5W ^{1}H irradiation concurrent with a ≈13 W MW irradiation. Larger ODNP enhancements (as measured by peak areas) could have been achieved if extending these irradiation times, yet the resolution of the ensuing spectra would have suffered unless extending even further the already long recycle delays used in this study. This would in turn compromise the sensitivity/unit_time performance of ODNP NMR; additional improvements in MW heating management are thus in progress in order to reap the full benefits of higher MW-driven enhancements. It is worth pointing out that temperature-gradient-driven NMR line broadenings are not uniform, and vary from compound to compound (e.g., chloroform's ^{13}C peak position is more sensitive to temperature than tetrachloromethane's) as well as from nucleus to nucleus. Hence, the acceptable degree of sample heating will vary depending on the specifics of the application. Also important to remark is the role of the solvent, whose dielectric losses will be the main determinants of the MW heating arising in large-volume DNP experiments; for instance, the experiments that were demonstrated here using essentially apolar solvents, would be impossible in absorbing solvents such as water, both because of sample heating and of limited MW penetration.

With these ^{13}C enhancements achieved, rINEPT-based $^{13}C \rightarrow {}^1H$ transfers were explored to port ODNP's polarization gains to the

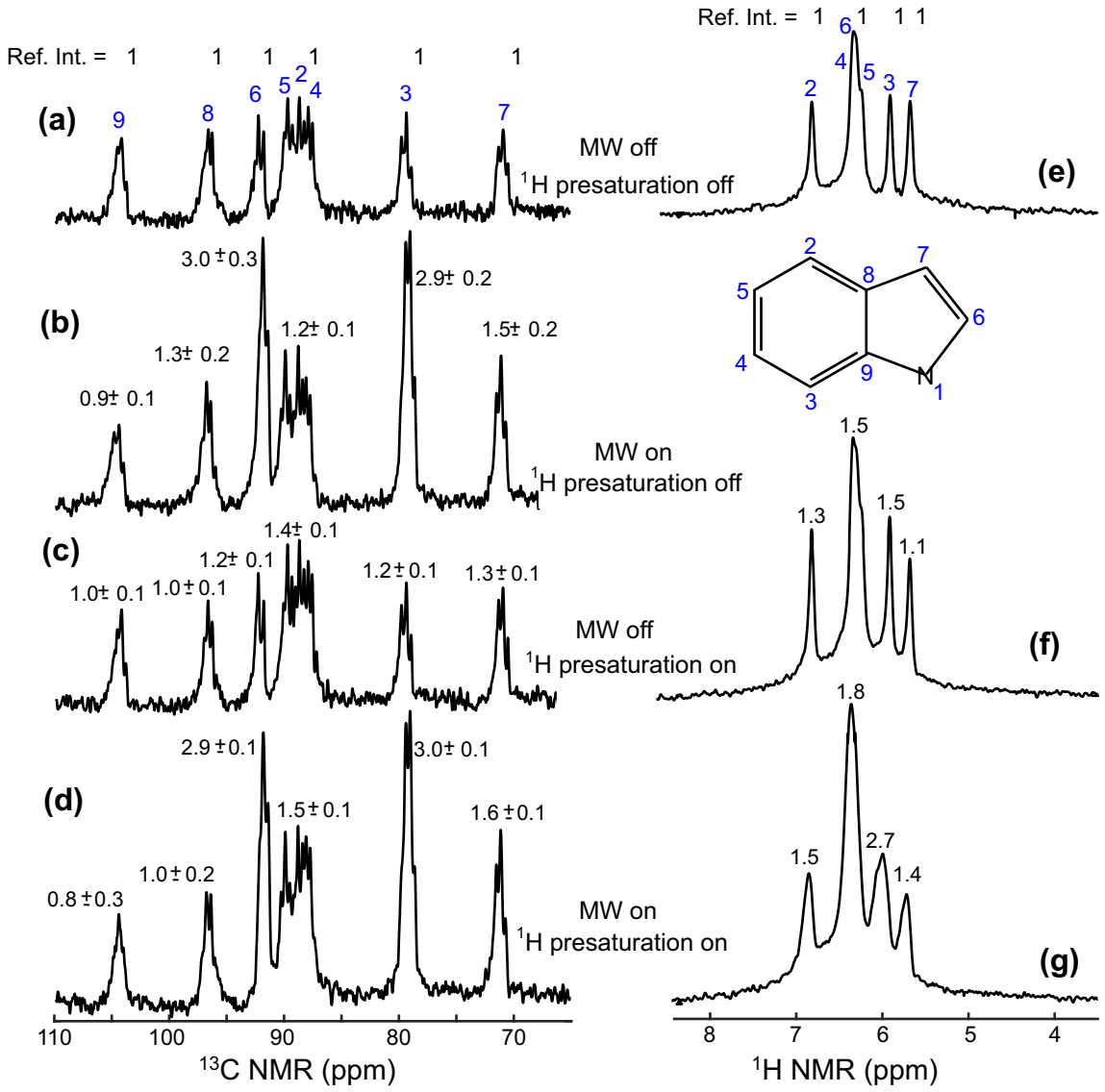

Fig. 6. Summary of ^{13}C (a-d) and ^{1}H (e-g) standard, NOE- and ODNP-enhanced NMR results measured on a 0.44 M $^{13}C_8$-indole, 10 mM TEMPO sample in 60 μL heptane-d_{16}/p-xylene-d_{10} (v/v = 4/1). All ^{13}C (left) and rINEPT ^{1}H (right column) spectra were taken with ^{1}H and ^{13}C decoupling, respectively. ^{1}H presaturation and MW irradiation were used as indicated; also indicated are the assignments of the peaks to the different sites in the molecule (labeled in the inset structure) and the relative intensities of the peaks vs heteronuclear-decoupled, thermal acquisition counterparts. Each ^{13}C / ^{1}H spectrum coadded 64 / 16 scans, respectively. d_1 and d_2 times used (cf. Fig. 2) were 5 and 2 s, respectively. The delay time 1/4J(^{1}H–^{13}C) used in the rINEPT sequences leading to the spectra in the right-hand column was determined by J(^{1}H–^{13}C) = 160 Hz. The chemical shifts of the ^{13}C and ^{1}H peaks were calibrated according to literature values [49]. Upon applying MW, the FWHH for the heteronuclear decoupled ^{1}H and ^{13}C peaks changed on average from 26 to 33 Hz and from 40 to 80 Hz, respectively.

more sensitive ^{1}H species. Such an approach is inherently of limited efficiency due to its reliance on transferring from a low- to a high-γ nucleus, yet it presents advantages and opportunities previously demonstrated for dissolution DNP methods –also a class of experiments feasible mostly on low-gamma nuclei. The signal increases that could then be observed in the ^{1}H spectra were near the expected maxima, and in all cases served to enhance the proton signals over their thermal counterparts. Further investigations are in progress to explore further uses of the ODNP enhancements achievable in these heteronuclear experiments, particularly in connection to extensions of ODNP-enhanced NMR to 2D heteronuclear correlations.

Another aspect explored in these multinuclear studies concerns the role of the ^{1}Hs and, in particular, of a concurrent ^{1}H saturation upon executing ODNP, on the polarization enhancement achieved by the ^{13}C. On thermal samples it was observed that the addition of a TEMPO radical (10 mM) to the solution under study, quenched the full-sized one-bond NOE effects that were otherwise present in a radical-free, deoxygenated counterpart. This is to a large degree expected, given the substantial paramagnetic relaxation competition brought about by the addition of the free radical –particularly of a free radical that will interact with the ^{13}C to later lead to an ODNP enhancement [23]. Interestingly, the ODNP enhancement changed negligibly upon concomitantly irradiating the ^{1}H that is in principle also involved in the formation of the transient species enabling the scalar-driven enhancement. This lends credence to the claim that the ^{1}H nucleus plays little or no significant role in facilitating the $e^- \rightarrow {}^{13}$C polarization transfer, and that this is dependent on direct electron radical spin density positioning at the carbon nucleus.

A final topic worth discussing concerns the roles that different moieties play in enabling the $e^- \rightarrow {}^{13}$C scalar interaction. It is speculated that protons attract radical electrons by forming a hydrogen-bonding-like interaction, thereby aiding to a closer con-

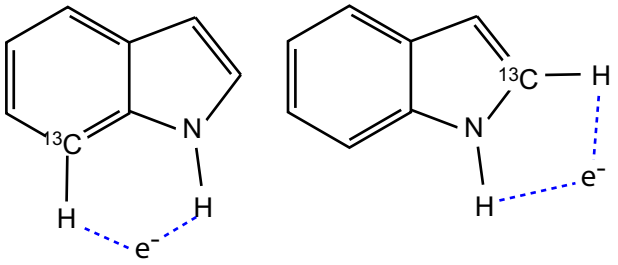

Scheme 1.

tact between the electron and ^{13}Cs [23,28,31]. This is consistent with the observation (Fig. 3) that $^{13}CHCl_3$, which contains a ^{1}H, shows a superior e^{-}-^{13}C ODNP enhancement effect than $^{13}CCl_4$ that does not contain any hydrogen. It is also consistent with the sites C3 and C6 showing the largest enhancements in indole (Fig. 6). These ^{13}C-^{1}Hs would be under favorable conditions for forming an e^{-}-^{13}C scalar coupling interaction by creating five- or six-membered ring complexes with the TEMPO radical electron; the hydrogen-bonding-like connections in these hypothetical rings could lead to $^{2}J(e^{-}$-$^{13}C)$-type scalar couplings (Scheme 1) favoring the ODNP. It is interesting to note, however, that despite being the closest ^{13}C from the amine group the quaternary site C9 does not show any noticeable e^{-}-^{13}C ODNP enhancement, remarking again the importance of having a hydrogen-bond-like structure in enabling these effects.

Data availability

Data will be made available on request.

Declaration of Competing Interest

The authors declare that they have no known competing financial interests or personal relationships that could have appeared to influence the work reported in this paper.

Acknowledgment

This work was performed at the National High Magnetic Field Laboratory, which is supported by the National Science Foundation (NSF) Cooperative Agreement No. DMR-1644779 and the state of Florida. SW's ODNP team acknowledges grant support from NSF (CHEM-2203405). LF holds the Bertha and Isadore Gudelsky Professorial Chair and Heads the Clore Institute for High-Field Magnetic Resonance Imaging and Spectroscopy at the Weizmann Institute; their support, as well as that of the Perlman Family Foundation, is acknowledged.

References

[1] A.W. Overhauser, Polarization of Nuclei in Metals, Phys. Rev. 92 (2) (1953) 411–415.
[2] T. Carver, Experimental Verification of the Overhauser Nuclear Polarization Effect, Phys. Rev. 102 (1956) 975–981.
[3] L.R. Becerra, G.J. Gerfen, R.J. Temkin, D.J. Singel, R.G. Griffin, Dynamic nuclear polarization with a cyclotron resonance maser at 5 T, Phys. Rev. Lett. 71 (21) (1993) 3561–3564.
[4] Maly, T.; Debelouchina, G. T.; Bajaj, V. S.; Hu, K.-N.; Joo, C., -G.; Mak Jurkauskas, M. L.; Sirigiri, J. R.; van der Wel, P. C. A.; Herzfeld, J.; Temkin, R. J.; Griffin, R. G., Dynamic nuclear polarization at high magnetic fields. *J. Chem. Phys.* **2008,** *128,* 052211.
[5] Q.Z. Ni, E. Daviso, T.V. Can, E. Markhasin, S.K. Jawla, T.M. Swager, R.J. Temkin, J. Herzfeld, R.G. Griffin, High Frequency Dynamic Nuclear Polarization, Accounts Chem. Res. 46 (9) (2012) 1933–1941.
[6] U. Akbey, W.T. Franks, A. Linden, S. Lange, R.G. Griffin, B.-J. Rossum, H. Oschkinat, Dynamic Nuclear Polarization of Deuterated Proteins, Angew. Chem. Int. Ed. 49 (2010) 7803–7806.
[7] J.H. Ardenkjaer-Larsen, F. Fridlund, A. Gram, G. Hansson, L. Hansson, M.H. Lerche, R. Servin, M. Thaning, K. Golman, Increase in signal-to-noise ratio of > 10,000 times in liquid-state NMR, Proc. Natl. Acad. Sci. USA 100 (2003) 10158–10163.
[8] K.M. Brindle, S.E. Bohndiek, F.A. Gallagher, M.I. Kettunen, Tumor imaging using hyperpolarized ^{13}C magnetic resonance spectroscopy, Magn. Reson. Med. 66 (2011) 505–519.
[9] S.J. Nelson, D. Vigneron, J. Kurhanewicz, A. Chen, R. Bok, R. Hurd, DNP-Hyperpolarized ^{13}C Magnetic Resonance Metabolic Imaging for Cancer Applications, Appl. Magn. Reson. 34 (2008) 533–544.
[10] J. Kurhanewicz, D.B. Vigneron, K. Brindle, E.Y. Chekmenev, A. Comment, C.H. Cunningham, R.J. DeBerardinis, G.G. Green, M.O. Leach, S.S. Rajan, R.R. Rizi, B.D. Ross, W.S. Warren, C.R. Malloy, Analysis of Cancer Metabolism by Imaging Hyperpolarized Nuclei: Prospects for Translation to Clinical Research, Neoplasia 13 (2011) 81–97.
[11] T. Harris, C. Bretschneider, L. Frydman, Dissolution DNP NMR with solvent mixtures: Substrate concentration and radical extraction, J. Magn. Reson. 211 (2011) 96–100.
[12] A. Bornet, R. Melzi, A.J.P. Linde, P. Hautle, B. van den Brandt, S. Jannin, G. Bodenhausen, Boosting Dissolution Dynamic Nuclear Polarization by Cross Polarization, Phys. Chem. Lett. 4 (2013) 111–114.
[13] S. Bowen, C. Hilty, Rapid sample injection for hyperpolarized NMR spectroscopy, Phys. Chem. Chem. Phys. 12 (2010) 5766–5770.
[14] A. Abragam, Overhauser Effect in Nonmetals, Phys. Rev. 98 (6) (1955) 1729–1735.
[15] I. Solomon, Relaxation Processes in a System of Two Spins, Phys. Rev. 99 (1955) 559–565.
[16] M.-T. Turke, M. Bennati, Comparison of Overhauser DNP at 0.34 and 3.4 T with Frémy's Salt, Appl. Magn. Reson. 43 (2012) 129–138.
[17] T. Orlando, R. Dervisoğlu, M. Levien, I. Tkach, T.F. Prisner, L.B. Andreas, V.P. Denysenkov, M. Bennati, Dynamic Nuclear Polarization of ^{13}C Nuclei in the Liquid State over a 10 Tesla Field Range, Angew. Chem. Int. Ed. 58 (5) (2019) 1402–1406.
[18] V.P. Denysenkov, T.F. Prisner, Liquid-State Overhauser DNP at High Magnetic Fields, eMagRes 8 (1) (2019) 14.
[19] S. van Meerten, High Sensitivity NMR in a Microfluidic Context, Radboud University, 2020.
[20] N.M. Loening, M. Rosay, V. Weis, R.G. Griffin, Solution-State Dynamic Nuclear Polarization at High Magnetic Field, J. Am. Chem. Soc. 124 (30) (2002) 8808–8809.
[21] D. Yoon, A.I. Dimitriadis, M. Soundararajan, C. Caspers, J. Genoud, S. Alberti, E. de Rijk, J.-P. Ansermet, High-Field Liquid-State Dynamic Nuclear Polarization in Microliter Samples, Anal. Chem. 90 (9) (2018) 5620–5626.
[22] V. Weis, M. Bennati, M. Rosay, J.A. Bryant, R.G. Griffin, High-Field DNP and ENDOR with a Novel Multiple-Frequency Resonance Structure, J. Magn. Reson. 140 (1999) 293–299.
[23] D. Dai, X. Wang, Y. Liu, X.-L. Yang, C. Glaubitz, V. Denysenkov, X. He, T.F. Prisner, J. Mao, Room-temperature dynamic nuclear polarization enhanced NMR spectroscopy of small biological molecules in water, Nat. Commun. 12 (2021) 6880.
[24] T. Dubroca, S. Wi, J. van Tol, L. Frydman, S. Hill, Large volume liquid state scalar Overhauser dynamic nuclear polarization at high magnetic field, Phys. Chem. Chem. Phys. 21 (2019) 21200–21204.
[25] C. Griesinger, M. Bennati, H.M. Vieth, C. Luchinat, G. Parigi, P. Höfer, F. Engelke, S.J. Glaser, V. Denysenkov, T.F. Prisner, Dynamic nuclear polarization at high magnetic fields in liquids, Prog. Nucl. Magn. Reson. Spectrosc. 64 (2012) 4–28.
[26] Wang, X.; Isley III, W. C.; Salido, S. I.; Sun, Z.; SOng, L.; Tsai, K. H.; Cramer, C. J.; Dorn, H. C., Optimization and prediction of the electron–nuclear dipolar and scalar interaction in ^{1}H and ^{13}C liquid state dynamic nuclear polarization. *Chem. Sci.* **2015,** *6,* 6482-6495.
[27] Dubroca, T.; Smith, A. N.; Pike, K., J.; Froud, S.; Wylde, R.; Trociewitz, B.; McKay, J.; Mentink-Vigier, F.; J., v. T.; Wi, S.; Brey, W.; Long, J. R.; Frydman, L.; Hill, S., A quasi-optical and corrugated waveguide microwave transmission system for simultaneous dynamic nuclear polarization NMR on two separate 14.1 T spectrometers. *J. Magn. Reson.* **2018,** *289*, 35-44.
[28] M. Bennati, C. Luchinat, G. Parigi, M.-T. Turke, Water ^{1}H relaxation dispersion analysis on a nitroxide radical provides information on the maximal signal enhancement in Overhauser dynamic nuclear polarization experiments, Phys. Chem. Chem. Phys. 12 (2010) 5902–5910.
[29] G. Liu, M. Levien, N. Karschin, G. Parigi, C. Luchinat, M. Bennati, One-thousand-fold enhancement of high field liquid nuclear magnetic resonance signals at room temperature, Nat. Chem. 9 (2017) 676–680.
[30] G. Parigi, E. Ravera, M. Bennati, C. Luchinat, Understanding Overhauser Dynamic Nuclear Polarisation through NMR relaxometry, Mol. Phys. 117 (2019) 888–897.
[31] T. Prisner, V. Denysenkov, D. Sezer, Liquid state DNP at high magnetic fields: Instrumentation, experimental results and atomistic modelling by molecular dynamics simulations, J. Magn. Reson. 264 (2016) 68–77.
[32] M. Mishkovsky, L. Frydman, Progress in Hyperpolarized Ultrafast 2D NMR Spectroscopy, ChemPhysChem 9 (2008) 2340–2348.
[33] R. Sarkar, A. Comment, P.R. Vasos, S. Jannin, R. Gruetter, G. Bodenhausen, H. Hall, D. Kirik, V.P. Denisov, Proton NMR of 15N-Choline Metabolites Enhanced by Dynamic Nuclear Polarization, J. Am. Chem. Soc. 131 (2009) 16014–16015.

[34] T. Harris, P. Giraudeau, L. Frydman, Kinetics from Indirectly Detected Hyperpolarized NMR Spectroscopy by Using Spatially Selective Coherence Transfers, Chem. Eur. J. 17 (2) (2011) 697–703.
[35] J. Wang, F. Kreis, A.J. Wright, R.L. Hesketh, M.H. Levitt, K.M. Brindle, Dynamic 1 H imaging of hyperpolarized [1-13 C]lactate in vivo using a reverse INEPT experiment, Magn. Reson. Med. 79 (2) (2018) 741–747.
[36] L. Frydman, D. Blazina, Ultrafast two-dimensional nuclear magnetic resonance spectroscopy of hyperpolarized solutions, Nature Phys 3 (2007) 415–419.
[37] E.Y. Chekmenev, V.A. Norton, D.P. Weitekamp, P. Bhattacharya, Hyperpolarized ^{1}H NMR Employing Low γ Nucleus for Spin Polarization Storage, J. Am. Chem. Soc. 131 (9) (2009) 3164–3165.
[38] P. Dzien, A. Fages, G. Jona, K.M. Brindle, M. Schwaiger, L. Frydman, Following Metabolism in Living Microorganisms by Hyperpolarized H-1 NMR, J. Am. Chem. Soc. 138 (37) (2016) 12278–12286.
[39] G.A. Morris, R. Freeman, Enhancement of nuclear magnetic resonance signals by polarization transfer, J. Am. Chem. Soc. 101 (3) (1979) 760–762.
[40] D.P. Burum, R.R. Ernst, Net polarization transfer via a J-ordered state for signal enhancement of low-sensitivity nuclei, J. Magn. Reson. 39 (1980) 163–168.
[41] S. Braun, H.-O. Kalinowski, S. Berger, 150 and More Basic NMR Experiments: A Practical Course, Weinheim, Germany, WILEY-VCH, 1998.
[42] Dubroca, T.; Scott, K.; Soundararajan, M.; McKay, J.; Trociewitz, B.; Hill, S.; van Tol, H.; Wi, S.; Frydman, L., High Efficiency Liquid Overhauser DNP Probe at 14.1 T. **2021**, Manuscript in preparation.
[43] X. Wang, W.C. Isley III, S.I. Salido, Z. Sun, L. Song, K.H. Tsai, C.J. Cramer, H.C. Dorn, Optimization and prediction of the electron-nuclear dipolar and scalar interaction in ^{1}H and ^{13}C liquid state dynamic nuclear polarization, Chem. Sci. 6 (2015) 6482–6495.
[44] T. Orlando, R. Dervişoğlu, M. Levien, I. Tkach, T.F. Prisner, L.B. Andreas, V.P. Denysenkov, M. Bennati, Dynamic nuclear polarization of C-13 nuclei in the liquid state over a 10 Tesla field range, Angew. Chem. Int. Ed. 58 (2019) 1402–1406.
[45] M. Levien, M. Hiller, I. Tkach, M. Bennati, T. Orlando, Nitroxide Derivatives for Dynamic Nuclear Polarization in Liquids: The Role of Rotational Diffusion, J. Phys. Chem. Lett. 11 (5) (2020) 1629–1635.
[46] A.J. Shaka, J. Keeler, T. Frenkiel, R. Freeman, An Improved Sequence for Broadband Decoupling: WALTZ-16, J. Magn. Reson. 52 (1983) 335–338.
[47] C. Szántay, Analysis and Implications of Transition-Band Signals in High-Resolution NMR, J. Magn. Reson. 135 (1998) 334–352.
[48] D. Neuhaus, M.P. Williamson, The Nuclear Overhauser Effect in Structural and Conformational Analysis, VCH Publishers Inc, New York, 1989.
[49] M.S. Morales-Rios, P. Joseph-Nathan, NMR Studies of Indoles and Their N-Carboalkoxy Derivatives, Magn. Reson. Chem. 25 (1987) 911–918.
[50] Y. Rao, A. Venkatesh, P. Moutzouri, L. Emsley, ^{1}H Hyperpolarization of Solutions by Overhauser Dynamic Nuclear Polarization with ^{13}C–^{1}H Polarization Transfer, J. Phys. Chem. Lett. 13 (2022) 7749–7755.